

Neutron skin effect in preequilibrium nucleon emissions

Sudip Ghosh and Maitreyee Nandy

Saha Institute of Nuclear Physics, 1/AF Bidhan Nagar, Calcutta 700064, India

P. K. Sarkar

H.P. Unit, Variable Energy Cyclotron Centre, 1/AF Bidhan Nagar, Calcutta 700064, India

N. Chakravarty

Nuclear Science Facility, San Jose State University, 1 Washington Square, San Jose, California 95192

(Received 5 October 1993)

The geometry-dependent hybrid model of preequilibrium nuclear reactions is used together with the droplet model description of neutron and proton densities to investigate the effect of excess surface neutrons on the nucleon emission spectra. It is found that in alpha-particle-induced reactions the effect of neutron skin on nucleon emission spectra is negligible. For nucleon-induced reactions the effect is more significant but not strong enough to remove the discrepancies between calculation and experiment.

PACS number(s): 21.10.Gv, 24.10.-i, 25.40.-h, 25.55.-e

I. INTRODUCTION

It is generally recognized that the existence of a diffuse nuclear surface will influence the emission spectra of particles at energies where the preequilibrium (PEQ) reaction mechanism is dominant. The energy spectra calculated without including surface effects in PEQ emissions usually underpredict the higher energy part of the spectra [1-3]. The diffuse nuclear surface affects the PEQ emissions in two ways. The two-body interaction rate decreases in the surface region on account of lower matter density resulting in enhancement of the emission probability. Also, the shallower potential well at the surface limits the hole energy which in turn increases the probability of particles occupying the higher energy states thereby increasing the higher energy emission probabilities. The two well-known models of PEQ reactions, the exciton model and the geometry-dependent hybrid (GDH) model, both include these effects for emissions from the early stages of the relaxation process. The exciton model incorporates the surface diffusivity effects through the parametrization of the effective well depth in the region of the first target-projectile interaction as a function of the incident energy [4]. The GDH model describes the nuclear density and potential by a two-parameter Fermi function and the diffuse surface effects arising at the higher impact parameters are included in the model calculations [5,6]. In addition to these two effects, a third effect of surface diffusivity, that of the effective neutron-skin in the neutron-rich targets, has also been investigated for PEQ nucleon emission by some authors [7,8]. In this work we reanalyze the effects of excess surface neutrons on the PEQ nucleon emission spectra. This reinvestigation is necessitated by the presence of numerical errors as well as inherent inconsistencies in the formalism of Ref. [8] and the absence of a reaction model analysis of the observations of Ref. [7]. The reaction

model formalism for including neutron skin is discussed in Sec. II and the results are presented in Sec. III.

II. NEUTRON SKIN IN PEQ REACTIONS

Castaneda *et al.* [8] made a model analysis of the neutron-skin effect on the measured inclusive proton spectra from $^{58,60,62,64}\text{Ni}(n,px)$ reactions at 60 MeV incident energy. The PEQ spectra were analyzed in terms of the hybrid and GDH models. The GDH calculations reproduced the spectral shapes better than the hybrid calculations but the former overpredicted the cross sections. To remove this discrepancy, the effect of neutron skin was introduced in the GDH model.

The GDH model PEQ energy spectra for ν -type nucleons is given by [6]

$$\sigma_{\text{PEQ}}(\epsilon) = \pi\lambda^2 \sum_{l=0}^{\infty} (2l+1)T_l \sum_{\substack{n=n_0 \\ \Delta n=2}}^{\bar{n}} D_n \left[{}_nX_{\nu} \frac{N_n(l, \epsilon, U)}{N_n(l, E)} \right] \times \frac{\lambda_c(\epsilon)}{\lambda_c(\epsilon) + \lambda_+(l, \epsilon)}, \quad (1)$$

where λ is the reduced de Broglie wavelength of the projectile and T_l the transmission coefficient of its l th partial wave. D_n is the depletion factor of the n th exciton state and ${}_nX_{\nu}$ is the number of ν -type excited nucleons in it. $N_n(l, E)$ is the number of ways in which n excitons share the excitation energy E and $N_n(l, \epsilon, U)$ is the number of ways in which the same energy E is distributed among the n excitons with one particle exciton having energy ϵ and the rest $(n-1)$ excitons sharing the energy U . $\lambda_c(\epsilon)$ and $\lambda_+(l, \epsilon)$ are, respectively, the emission and two-body collision rates. The significance of the various terms are discussed in Ref. [6].

In (1) the cross sections are evaluated for each impact parameter $r_l = l\lambda$ and the diffuse surface properties show up at larger impact parameters. The lower matter density at the surface decreases $\lambda_+(l, \epsilon)$ while the shallower surface potential enhances the ratio $N_n(\epsilon, l, U)/N_n(l, E)$ which is the probability of finding a nucleon with emission energy ϵ . The effect of neutron skin is introduced in ${}_nX_\nu$ which is independent of r_l if protons and neutrons are assumed to be uniformly distributed inside the nucleus. Otherwise, it is a function of proton and neutron density distributions, $\rho_p(r_l)$ and $\rho_n(r_l)$, respectively.

For nucleon projectile the initial exciton number $n_0 = 3$ and ${}_nX_n + {}_nX_p = 2$. In the GDH (and hybrid) model the number of excited neutrons in the n_0 state is evaluated as [6]

$${}_3X_n = \frac{3Z + 2N}{3Z + N} \quad (2)$$

for a neutron projectile and

$${}_3X_n = \frac{3N}{3N + Z} \quad (3)$$

for a proton projectile. Z and N are the proton and neutron numbers, respectively, of the target. These initial values of ${}_nX_n$ and ${}_nX_p$ are each assumed to increase by 0.5 in successive values of n . The effect of neutron skin is introduced in [8] by replacing Z , N by $\rho_p(r_l)$, $\rho_n(r_l)$ respectively, to get

$${}_3X_n = \frac{3\rho_p(r_l) + 2\rho_n(r_l)}{3\rho_p(r_l) + \rho_n(r_l)}, \quad (4)$$

$${}_3X_n = \frac{3\rho_n(r_l)}{3\rho_n(r_l) + \rho_p(r_l)}, \quad (5)$$

for neutron and proton projectiles, respectively.

A. Parametrization of densities

The neutron and proton density distributions are taken as

$$\rho_\nu(r) = \frac{\rho_{0\nu}}{1 + \exp[(r - R_\nu)/\alpha_\nu]} \quad (6)$$

In Ref. [8] the half-density radii R_ν are defined as

$$R_p = 1.18A^{\frac{1}{3}} \left[1 - \frac{1}{(1.18A^{\frac{1}{3}})^2} \right] + \lambda, \quad (7)$$

$$R_n = R_p + t. \quad (8)$$

The neutron-skin thickness t is defined from the droplet model (DM) [10,11]. It is further assumed in Ref. [8] that $\rho_{0p} = \rho_{0n}$ and the diffusivity constants $\alpha_p = \alpha_n = 0.55$ fm.

With this parametrization of ${}_nX_\nu$, it is reported [8] that the overpredictions in proton emission cross sections are corrected and good agreement is obtained between experiment and GDH calculations. On repeating the calculations, however, we find that, contrary to what has been reported, the decrease in proton emission cross sections on account of including the neutron-skin effect is very small as shown in Fig. 1. Numerical errors in the calculations of Ref. [8] are responsible for the reported large decrease in the proton emission cross sections. The skin thickness algorithm in Ref. [8] was most likely encoded with an incorrect numerical constant, such as to give a neutron skin thickness in error by a factor of 10 [9].

In addition to the numerical errors, the parametrization of $\rho_p(r_l)$, $\rho_n(r_l)$ of (6) as described in Ref. [8] suffers from the shortcoming that particle number conservation, given by

$$A = Z + N = 4\pi \left[\int_0^\infty r^2 \rho_p(r) dr + \int_0^\infty r^2 \rho_n(r) dr \right], \quad (9)$$

is not taken into account. If it is assumed that R_p is given by (7), $\rho_{0p} = \rho_{0n}$, $\alpha_p = \alpha_n = 0.55$ fm, and R_n is obtained from the number conservation of N from (9), then the value $t = R_n - R_p$ is different from the DM values of t .

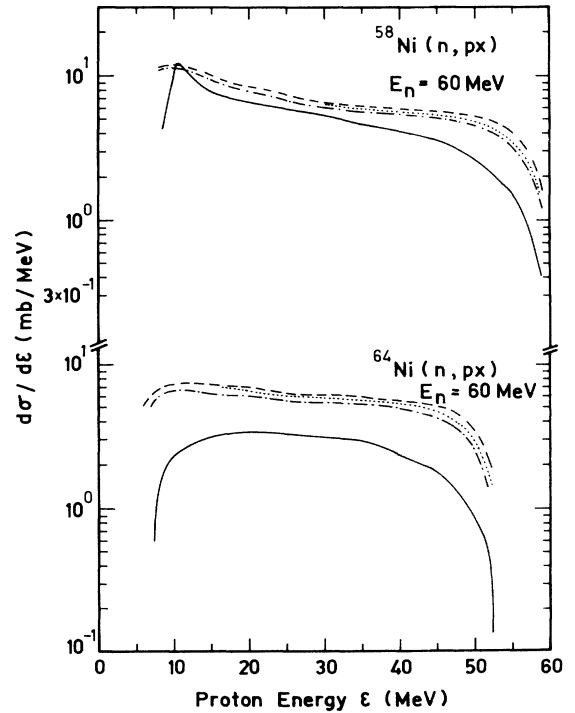


FIG. 1. Experimental and calculated proton spectra from ${}^{58,64}\text{Ni}(n, px)$ reactions at 60 MeV neutron energy. The solid curves are the experimental results from Ref. [8]. The dashed curves are the GDH+hybrid model calculations without neutron skin. The dotted and dashed-dotted curves are calculated with neutron skin; the former use the density parameters of Ref. [8] and the latter the present work.

On the other hand, t being an important variable of the DM, the definitions of $\rho_{0p}, \rho_{0n}, R_p, R_n, \alpha_p$, and α_n must be consistent with the DM and (9).

B. The droplet model description of densities

The DM [10,11] is a refinement of the liquid drop model (LDM). In the LDM the proton and neutron densities are constant inside a sharp boundary and zero outside. In the DM the densities are only approximately constant in the bulk of the system and smoothly decrease to zero through a diffuse surface region. The density nonuniformities in the bulk region and the thickness of the surface region are treated as small quantities and the DM defines average proton and neutron densities $\bar{\rho}_p$ and $\bar{\rho}_n$ in the bulk region that are close to the radius-dependent densities. Corresponding to $\bar{\rho}_p$ and $\bar{\rho}_n$ the DM also defines sharp boundaries R_{0p} and R_{0n} for the proton and neutron distributions. From number conservation

$$Z = \frac{4}{3}\pi R_{0p}^3 \bar{\rho}_p, \quad (10)$$

$$N = \frac{4}{3}\pi R_{0n}^3 \bar{\rho}_n. \quad (11)$$

The deviation of the average matter density $\bar{\rho} = \bar{\rho}_p + \bar{\rho}_n$ from the constant LDM density ρ_{LDM} is defined in terms of the dimensionless quantity

$$\bar{\epsilon} = -\frac{1}{3} \frac{\bar{\rho} - \rho_{\text{LDM}}}{\rho_{\text{LDM}}}, \quad (12)$$

where $\rho_{\text{LDM}} = (4\pi r_0^3/3)^{-1}$, r_0 being the nucleon radius. The DM also defines a density asymmetry parameter

$$\bar{\delta} = \frac{\bar{\rho}_n - \bar{\rho}_p}{\bar{\rho}}. \quad (13)$$

From (10) to (13)

$$\bar{\rho}_p = \frac{1}{2}\bar{\rho}(1 - \bar{\delta}), \quad (14)$$

$$\bar{\rho}_n = \frac{1}{2}\bar{\rho}(1 + \bar{\delta}), \quad (15)$$

$$R_{0p} = r_0 \left[\frac{2Z}{(1 - 3\bar{\epsilon})(1 - \bar{\delta})} \right]^{1/3}, \quad (16)$$

$$R_{0n} = r_0 \left[\frac{2N}{(1 - 3\bar{\epsilon})(1 + \bar{\delta})} \right]^{1/3}. \quad (17)$$

The DM defines $\bar{\delta}$ and $\bar{\epsilon}$ in terms of six constants which are determined from variational calculations. From the expressions of $\bar{\delta}$ and $\bar{\epsilon}$ in Ref. [11], $\bar{\rho}_p, \bar{\rho}_n, R_{0p}$, and R_{0n} can be evaluated. The neutron-skin thickness is defined as

$$t = R_{0n} - R_{0p} \approx \frac{3}{2}r_0 \frac{4J(N - Z) - (CZA^{2/3})/3}{4QA^{2/3} + 9JA^{2/3}}, \quad (18)$$

where the symmetry energy coefficient $J = 36.8$ MeV, the effective surface stiffness coefficient $Q = 17$ MeV, and the Coulomb coefficient $C = 0.73$ MeV with $r_0 = 1.18$ fm [10,11].

The DM density distributions can be approximated by a two-parameter Fermi function (6) as has been done by Myers [11] for comparing the DM sharp radius, R_{0p} , with experimental charge distribution which is conveniently represented by a two- or three-parameter function. Since

TABLE I. Calculated values of density parameters of Eq. 6. ρ_{0n} and ρ_{0p} are in fm^{-3} and the other parameters are in fm. Values of α_p are from Ref. [13]. The parameters in the second line for each nucleus corresponds to $\rho_{0p} = \rho_{0n}$.

Nucleus	ρ_{0p}	ρ_{0n}	R_{0p}	R_{0n}	t	α_p	α_n	R_p	R_n
^{58}Ni	0.0782	0.0818	4.404	4.441	0.037	0.560	0.579	4.156	4.193
	0.0800	0.0800	4.371	4.473	0.102	0.560	0.584	4.120	4.222
^{64}Ni	0.0747	0.0846	4.473	4.665	0.192	0.578	0.609	4.212	4.404
	0.0800	0.0800	4.371	4.753	0.382	0.578	0.622	4.103	4.485
^{112}Sn	0.0722	0.0818	5.486	5.656	0.170	0.560	0.579	5.291	5.461
	0.0774	0.0774	5.363	5.761	0.398	0.560	0.592	5.163	5.561
^{118}Sn	0.0703	0.0833	5.538	5.797	0.259	0.583	0.608	5.328	5.587
	0.0774	0.0774	5.361	5.940	0.579	0.583	0.627	5.144	5.723
^{120}Sn	0.0696	0.0838	5.555	5.842	0.287	0.576	0.602	5.351	5.638
	0.0775	0.0775	5.361	5.997	0.636	0.576	0.622	5.148	5.784
^{124}Sn	0.0684	0.0846	5.589	5.932	0.343	0.539	0.564	5.412	5.755
	0.0775	0.0775	5.360	6.108	0.748	0.539	0.586	5.175	5.923
^{208}Pb	0.0646	0.0832	6.717	7.121	0.404	0.549	0.572	6.567	6.971
	0.0754	0.0754	6.379	7.361	0.982	0.549	0.597	6.220	7.202

ρ_{0p}, ρ_{0n} of (6) remain approximately constant in the bulk region we define $\rho_{0p} = \bar{\rho}_p$ and $\rho_{0n} = \bar{\rho}_n$.

The parameters R_p, R_n, α_p , and α_n are obtained from (9) which, under the conditions $\alpha_p \ll R_p, \alpha_n \ll R_n$, can be reduced to the well-known approximate forms [12]:

$$Z \approx \frac{4}{3} \pi \rho_{0p} R_p^3 \left(1 + \frac{\pi^2 \alpha_p^2}{R_p^2} \right), \quad (19)$$

$$N \approx \frac{4}{3} \pi \rho_{0n} R_n^3 \left(1 + \frac{\pi^2 \alpha_n^2}{R_n^2} \right). \quad (20)$$

Equating (10) and (11) with (19) and (20),

$$R_{0p}^3 = R_p^3 \left(1 + \frac{\pi^2 \alpha_p^2}{R_p^2} \right), \quad (21)$$

$$R_{0n}^3 = R_n^3 \left(1 + \frac{\pi^2 \alpha_n^2}{R_n^2} \right). \quad (22)$$

Since the four unknown parameters cannot be solved from (21) and (22) only, we estimate R_p from (21) using experimental values of α_p obtained from fitting electron scattering form factors by a two-parameter Fermi function [13]. To evaluate R_n we note that under the conditions $\alpha_p \ll R_p, \alpha_n \ll R_n$ we may write

$$R_n - R_p \approx R_{0n} - R_{0p} = t. \quad (23)$$

α_n can then be obtained from (22).

The calculated values of the parameters defining $\rho_p(r)$ and $\rho_n(r)$ together with the experimental values of α_p used are given in Table I. Calculated values of the same parameters under the assumption $\rho_{0n} = \rho_{0p}$ ($\bar{\delta} = 0$) are also given. This results in a thicker neutron skin—almost double the value obtained with $\rho_{0n} \neq \rho_{0p}$. The assumption $\rho_{0n} = \rho_{0p}$, however, is not consistent with the DM definition of t . The formation of neutron skin results from two opposing effects. The neutron excess tends to produce a neutron skin while Coulomb repulsion between protons tends to reduce it by requiring extra neutrons in the bulk region to compensate for Coulomb repulsion [10]. This latter effect is responsible for $\rho_{0n} > \rho_{0p}$ and the assumption $\rho_{0n} = \rho_{0p}$ implies negating the Coulomb repulsion between protons.

III. RESULTS AND DISCUSSIONS

A. Nucleon-induced reactions

The calculations are performed with the code ALICE [14] which was modified to include neutron-skin effect through (4) and (5). The GDH calculations are restricted to the initial exciton state $n_0 = 3$. Emissions from higher exciton states are calculated by the hybrid model. All input parameters are generated internally as described in Ref. [6]. The optical model option has been used to calculate the inverse reaction cross sections. The parameters

are tabulated in Ref. [6]. The same parameters also calculate the partial reaction cross sections, $\sigma_l = \pi \lambda^2 (2l+1) T_l$. The two-body interaction rates, $\lambda_+(l, \epsilon)$, are evaluated from nucleon mean free paths calculated from Pauli corrected nucleon-nucleon scattering cross sections instead of from the optical model. This also is discussed in Ref. [6]. In the present code there is an important deviation from the parametrization of Ref. [6] related to the emission rate $\lambda_c(\epsilon)$. In Ref. [6] $\lambda_c(\epsilon)$ is calculated using energy-dependent proton and neutron single particle level densities, g_p and g_n , respectively. This is, however, inconsistent with the evaluation of $N_n(l, \epsilon, U)/N_n(l, E)$ of (1) where energy-independent g_p and g_n are used. This ratio is the probability of finding a particle-exciton with energy ϵ in the n -exciton state prior to emission. Since it is improper to describe the same energy state by both energy-dependent and energy-independent g_p and g_n , the present code [14] uses constant $g_p (= Z/14)$ and $g_n (= N/14)$ to calculate $\lambda_c(\epsilon)$ instead of the energy-dependent expression of Ref. [6].

The proton emission spectra from the $^{58,64}\text{Ni}(n, px)$ reaction at 60 MeV incident energy calculated with (4) and (6) using the DM defined parameters of $\rho_p(r)$ and $\rho_n(r)$ are shown in Fig. 1. The decrease in proton emission cross sections is more pronounced with the present set of parameters than with the earlier ones of Ref. [8]. But the decrease is not large enough to compensate for the over-prediction of GDH model calculations without the effect of neutron skin. To see if the effect of neutron skin is enhanced for targets with larger neutron excess we have calculated the inclusive neutron spectra from $^{120}\text{Sn}(p, n)$ and $^{208}\text{Pb}(p, n)$ reactions at 45 MeV incident energy with (3) and (5) defining $n_0 X_\nu$ (proton projectile). The results are compared with experiment [2] in Fig. 2. The neutron emission cross sections calculated with (3) (no neutron

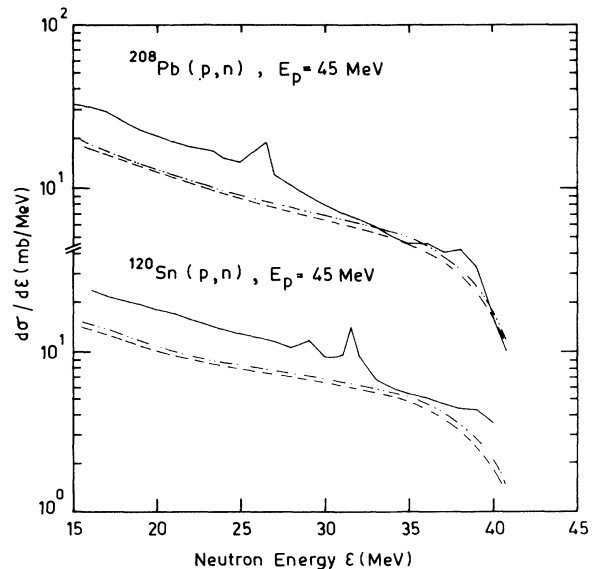


FIG. 2. Experimental and calculated neutron spectra from $^{208}\text{Pb}(p, n)$ and $^{120}\text{Sn}(p, n)$ reactions at 45 MeV proton energy. The experimental results (solid curves) are from Ref. [2]. The calculated curves are the same as in Fig. 1.

skin) underpredict the experimental values. The inclusion of neutron skin through (5) does enhance the cross sections, as expected, but not strongly enough to remove the discrepancy between calculation and experiment. We also calculated the nucleon emission spectra for these reactions with the assumption $\rho_{0n} = \rho_{0p}$ ($\bar{\delta} = 0$). Although this implies ignoring the Coulomb repulsion between protons (Sec. II B), it results in considerably thicker neutron skin (Table I). The change in cross sections with respect to the calculations with $\bar{\delta} \neq 0$, however, is insignificant. The reason is evident from Fig. 3 which shows the variation of l with partial reaction cross section σ_l and the ratio $n_0 X_n / n_0 X_p$ for the $^{208}\text{Pb}(p, n)$ reaction at 45 MeV. At high impact parameters $r_l (= l\lambda)$, where the neutron skin becomes prominent, σ_l is so small that a change in $n_0 X_n$ does not significantly alter the emission cross sections.

B. Alpha-particle-induced reactions

Fields *et al.* [7] measured the exclusive neutron spectra of $(\alpha, 2n\gamma)$ reactions from several targets at varying projectile energies. Among other results, they observed that the square of the ratio of the peak of the PEQ component to that of the equilibrium (EQ) component of the spectra showed a rising trend with (a) $tA^{1/3}$, a quantity proportional to the annular cross-sectional area of the neutron skin, and (b) the available energy, $E_\alpha + Q$, of neutron emission— Q being the Q value of the $(\alpha, 2n\gamma)$ reaction and E_α the center-of-mass projectile energy. Comparison of the PEQ to EQ ratios at fixed $E_\alpha + Q$ showed pronounced increase with $tA^{1/3}$. This was attributed to the enhancement of PEQ neutron emission from the neutron-skin region of the target. No reaction model calculation was presented for this observation. We use the GDH model to analyze this feature. GDH model calculations in

Ref. [7] of the angle-integrated, inclusive neutron spectra from the $^{112,118,124}\text{Sn}(\alpha, 2n\gamma)$ reactions reproduced the shapes of the spectra quite well. The calculations were done with an earlier version of GDH model in which PEQ emissions were limited to single nucleons. In the present calculations with the code ALICE [14], both single- and two-nucleon PEQ emissions are taken into account. To define n_0 and $n_0 X_\nu$ of (1), we note that of the several ways in which an alpha projectile can be removed from the entrance channel [15], the most important are (a) the complete dissolution of the projectile into its constituent nucleons and (b) creation of a particle-hole (p-h) pair. In (a) the initial state is a 4p-0h configuration with $n_0 = 4$, $n_0 X_n = n_0 X_p = 2$, and the target properties are irrelevant for defining $n_0 X_\nu$. Reference [7] used these values of n_0 and $n_0 X_\nu$. In (b) a 5p-1h state is formed with $n_0 = 6$ and $n_0 X_n + n_0 X_p = 5$. We define

$$n_0 X_n = 2 + \frac{N}{N + Z}. \quad (24)$$

To investigate the effect of local variations of neutrons and protons, the local densities replace N and Z as in the nucleon-induced reactions:

$$n_0 X_n = 2 + \frac{\rho_n(r_l)}{\rho_n(r_l) + \rho_p(r_l)}. \quad (25)$$

The calculated spectra (with the same input parameters as in nucleon induced reactions except that the code calculates σ_l for alpha projectiles from the Hill-Wheeler expression for the penetrability of a parabolic barrier) are compared with the experimental results of Ref. [7] in Fig. 4. The shapes of the spectra are satisfactorily reproduced with $n_0 = 4$ while $n_0 = 6$ underpredicts the higher energy emissions. An admixture of $n_0 = 4$ and 6 should be used for alpha-particle-induced reactions as suggested in Ref. [15]. More pertinent to the present investigation is the almost insignificant increase in neutron emission after inclusion of neutron skin through (25). This very small effect of the neutron skin in alpha-particle-induced reactions, as compared to nucleon-induced reactions, can be understood by the presence of two protons in the alpha-particle which dilutes the effect of the increased number of excited neutrons in the neutron-skin region for the n_0 exciton state.

We now make a GDH model analysis of the observation of Ref. [7] that the ratio of the PEQ to EQ components of the neutron spectra increases with $tA^{1/3}$ at fixed $E_\alpha + Q$. In $(\alpha, 2n\gamma)$ reactions the residual nucleus can be formed through the following three channels. *Channel 1*: simultaneous PEQ emission (from the same exciton state) of two neutrons from the target+projectile composite nucleus (Z_c, A_c) ; *channel 2*: PEQ neutron emission from (Z_c, A_c) followed by EQ neutron emission from the intermediate nucleus $(Z_c, A_c - 1)$; and *channel 3*: two successive EQ neutron emissions from (Z_c, A_c) and $(Z_c, A_c - 1)$. There is a fourth possible channel in which two successive PEQ neutrons may be emitted from (Z_c, A_c) and $(Z_c, A_c - 1)$ but since the GDH model considers only single- and simultaneous two-nucleon PEQ emissions from (Z_c, A_c) [6] contributions from this channel are neglected in the present calculations.

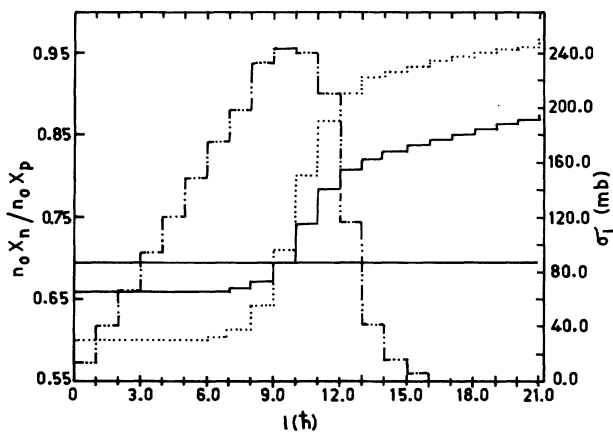


FIG. 3. Variation of the ratio $n_0 X_n / n_0 X_p$ (left vertical axis) with entrance channel orbital angular momentum l for the $^{208}\text{Pb}(p, n)$ reaction at 45 MeV incident energy. The full line is the value obtained without neutron skin. The solid histogram represents the case for $\rho_{0n} \neq \rho_{0p}$ and the dotted histogram for $\rho_{0n} = \rho_{0p}$. Also shown (dash-dotted histogram) is the variation of the partial reaction cross section σ_l , (right vertical axis).

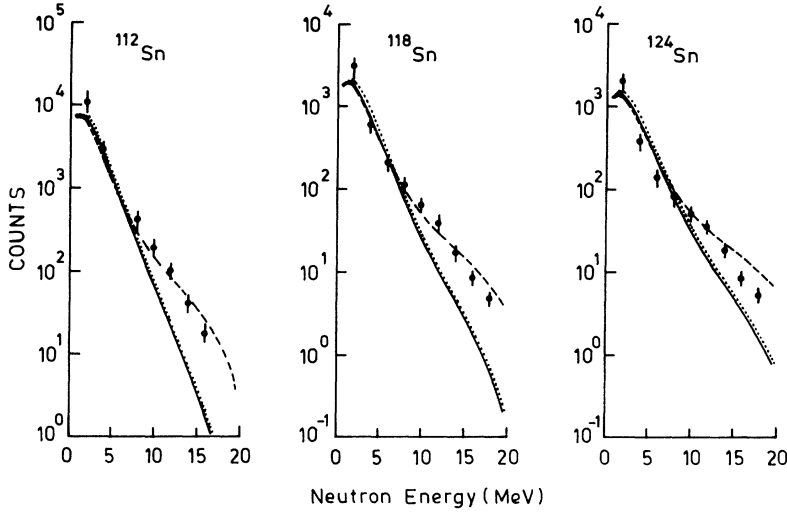


FIG. 4. Comparison of experimental and calculated angle-integrated neutron spectra from $^{112,118,124}\text{Sn}(\alpha, 2n)$ reactions at 35 MeV incident energy. The experimental points are from Ref. [7]. The dashed curves are the calculations with $n_0 = 4$ (no neutron skin.) The dotted and solid curves are calculated for $n_0 = 6$ with and without neutron skin, respectively.

If $N_{\text{PEQ}}(1)$ and $N_{\text{PEQ}}(2)$ are the number of PEQ neutrons emitted in channels 1 and 2, respectively, and $N_{\text{EQ}}(2)$ and $N_{\text{EQ}}(3)$ are the number of EQ neutrons in channels 2 and 3, respectively, then the total number of PEQ neutrons $N_{\text{PEQ}} = N_{\text{PEQ}}(1) + N_{\text{PEQ}}(2)$ and the total number of EQ neutrons $N_{\text{EQ}} = N_{\text{EQ}}(2) + N_{\text{EQ}}(3)$. Also, if σ_1 , σ_2 , and σ_3 are the formation cross sections of the residual through channels 1, 2, and 3, respectively, then $N_{\text{PEQ}}(1) \propto \sigma_1$, $N_{\text{PEQ}}(2) + N_{\text{EQ}}(2) \propto \sigma_2$, and $N_{\text{EQ}}(3) \propto \sigma_3$. Again, $N_{\text{PEQ}}(2) = N_{\text{EQ}}(2)$ since each PEQ neutron emission in channel 2 is followed by one EQ neutron emission. We then have

$$\frac{N_{\text{PEQ}}}{N_{\text{EQ}}} = \frac{\sigma_1 + \frac{1}{2}\sigma_2}{\sigma_3 + \frac{1}{2}\sigma_2}, \quad (26)$$

as the ratio of the numbers of PEQ to EQ neutrons in $(\alpha, 2n\gamma)$ reactions. The cross sections σ_1 , σ_2 , and σ_3 are obtained from GDH+hybrid+EQ calculations using the code ALICE. Once again the GDH model calculations are restricted to n_0 and PEQ emissions from higher exciton states are calculated by the hybrid model.

The results of the calculations with $n_0 = 4$ (no neutron skin) are shown in Fig. 5 where $N_{\text{PEQ}}/N_{\text{EQ}}$ is plotted as a function of $tA^{1/3}$. The overall rising trend of $N_{\text{PEQ}}/N_{\text{EQ}}$ even without explicit inclusion of neutron skin reflects the relative increase of PEQ neutrons with the overall neutron excess ($N - Z$) rather than neutron skin—the dominant term in the evaluation of t from (18) being $4J(N - Z)/A$. The dependence of $N_{\text{PEQ}}/N_{\text{EQ}}$ on the neutron excess comes in through the interplay of projectile and ejectile separation energies as was suggested by Betak and Dobes [16].

The ratio $N_{\text{PEQ}}/N_{\text{EQ}}$ is determined mainly by the relative contributions from channels 2 and 3 since contribution from channel 1 is small. In both these channels the intermediate nucleus ($Z_c, A_c - 1$) is formed with maximum possible excitation $U_{\text{max}} = E_\alpha + S_\alpha(Z_c, A_c) - S_n(Z_c, A_c)$, where $S_\alpha(Z_c, A_c)$ and $S_n(Z_c, A_c)$ are the alpha-particle and neutron separation energies in the composite nucleus (Z_c, A_c). U_{max} shows a generally de-

creasing trend with $tA^{1/3}$, i.e., with increasing neutron excess, at fixed $E_\alpha + Q$ as is shown in Fig. 5. The residual nucleus is formed through EQ neutron emission from an excitation energy U of $(Z_c, A_c - 1)$, where $U = U_{\text{max}} - \epsilon$, ϵ being the energy of the first neutron. The PEQ and EQ cross sections, $\sigma_{\text{PEQ}}(\epsilon)$ and $\sigma_{\text{EQ}}(\epsilon)$ populating a given U are determined by ϵ and U_{max} . In the evaporation approximation (sharp cutoff inverse cross section) of EQ

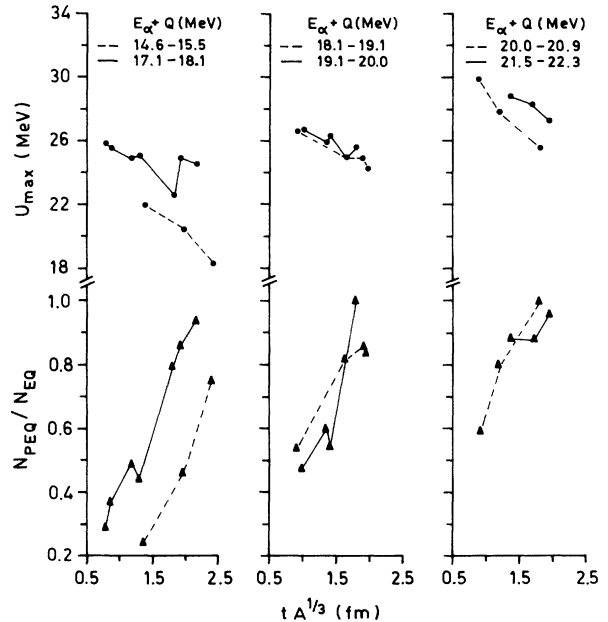


FIG. 5. Variation of $N_{\text{PEQ}}/N_{\text{EQ}}$, the calculated ratio of the number of PEQ to EQ neutrons with $tA^{1/3}$ for $E_\alpha + Q$ fixed within 1 MeV from $(\alpha, 2n\gamma)$ reactions on ^{85}Rb , ^{89}Y , ^{90}Zr , $^{104,106,108,110}\text{Pd}$, $^{112,118,120,124}\text{Sn}$, ^{139}La , $^{148,150}\text{Nd}$, ^{165}Ho , ^{197}Au , and ^{208}Pb (Ref. [7]). The variation of U_{max} , the maximum possible excitation energy available after one neutron emission, is shown in the upper part of the figure. The lines connect the points belonging to a given $E_\alpha + Q$ energy bin.

emission

$$\sigma_{EQ}(\epsilon) \sim \epsilon \exp(-\epsilon/T), \quad (27)$$

where the temperature parameter $T \propto \sqrt{U_{\max}}$ [17]. For a given ϵ (i.e., for a given U) $\sigma_{EQ}(\epsilon)$ decreases exponentially with decreasing $\sqrt{U_{\max}}$. The PEQ cross section $\sigma_{PEQ}(\epsilon) = \sum_n \sigma_n(\epsilon)$, where $\sigma_n(\epsilon)$ is the neutron emission cross section from the exciton state n . With the sharp cutoff inverse cross section and the partial level densities of Ericson [17] $\sigma_n(\epsilon)$ from (1) can be written as

$$\begin{aligned} \sigma_n(\epsilon) &\sim \epsilon \frac{N_n(\epsilon, U)}{N_n(E)} \sim (n-1)\epsilon U^{n-2} \\ &\sim (n-1)\epsilon(U_{\max} - \epsilon)^{n-2}. \end{aligned} \quad (28)$$

$\sigma_{PEQ}(\epsilon)$ also decreases with U_{\max} but less rapidly than $\sigma_{EQ}(\epsilon)$ as can be seen from (27) and (28). Hence, with decreasing U_{\max} , N_{EQ} decreases faster than N_{PEQ} which results in the observed overall increase of N_{PEQ}/N_{EQ} with increasing $tA^{1/3}$ as U_{\max} decreases with $tA^{1/3}$.

IV. SUMMARY

We have investigated the effect of neutron skin in PEQ emissions using the GDH model with the droplet model

description of proton and neutron densities in terms of two-parameter Fermi functions. We have found that in alpha-particle-induced reactions the effect of neutron skin is insignificant. This is primarily because the presence of two protons in the projectile masks the effect of excess neutrons in the surface region.

For nucleon-induced reactions the effect is stronger but still not very significant. The reason is the rapid decrease of partial reaction cross sections in the surface region where the neutron-skin is pronounced. This is attributable to the phenomenological optical model potential [6] used in the calculations which is unrelated to the proton and neutron distributions evaluated from the DM. In this connection it would be interesting to investigate whether the neutron-skin effect is enhanced if, instead of a phenomenological optical potential, microscopic folding model calculations [18] with the DM density distributions are used to evaluate the partial reaction cross sections.

ACKNOWLEDGMENTS

The authors are thankful to Professor M. Blann of the Lawrence Livermore National Laboratory for many helpful discussions and suggestions.

-
- [1] J.R. Wu and C.C. Chang, *Phys. Lett.* **60B**, 423 (1976); J.R. Wu, C.C. Chang, and H.D. Holmgren, *Phys. Rev. C* **19**, 698 (1977).
 - [2] M. Blann, R.R. Doering, A. Galonsky, D.M. Patterson, and F.E. Serr, *Nucl. Phys.* **A257**, 15 (1976).
 - [3] C. Kalbach, *Z. Phys. A* **238**, 401 (1977).
 - [4] C. Kalbach, *Phys. Rev. C* **32**, 1157 (1985).
 - [5] M. Blann, *Phys. Rev. Lett.* **28**, 757 (1972); *Nucl. Phys.* **A213**, 570 (1973).
 - [6] M. Blann and H.K. Vonach, *Phys. Rev. C* **28**, 1475 (1983).
 - [7] C.A. Fields, F.W.N. De Boer, R.A. Ristinen, P.A. Smith, and E. Sugarbaker, *Nucl. Phys.* **A377**, 217 (1982).
 - [8] C.M. Castaneda, J.L. Ullmann, F.P. Brady, J.L. Romero, N.S.P. King, and M. Blann, *Phys. Rev. C* **28**, 1493 (1983).
 - [9] M. Blann (private communication).
 - [10] W.D. Myers and W.J. Swiatecki, *Ann. Phys. (N.Y.)* **55**, 395 (1969); **84**, 186 (1974).
 - [11] W.D. Myers, *Droplet Model of Atomic Nuclei* (Plenum, New York, 1977).
 - [12] J.E. Mayer and M.G. Mayer, *Statistical Physics* (Wiley, New York, 1977), Chap. 11.
 - [13] C.W. de Jager, H. de Vries, and C. de Vries, *At. Data Nucl. Data Tables* **14**, 479 (1974).
 - [14] M. Blann, Lawrence Livermore National Laboratory Report No. UCID 20169, 1984 (unpublished).
 - [15] E. Gadioli, E. Gadioli-Erba, J.J. Hogan, and B.V. Jacak, *Phys. Rev. C* **29**, 76 (1984).
 - [16] E. Betak and J. Dobes, *Phys. Lett.* **130B**, 350 (1983).
 - [17] T. Ericson, *Adv. Phys.* **9**, 425 (1960).
 - [18] G.R. Satchler and W.G. Love, *Phys. Rep.* **55**, 183 (1979).